

First Demonstration of a Silicon-Organic Hybrid (SOH) Modulator Based on a Long-Term-Stable Crosslinked Electro-Optic Material

A. Schwarzenberger^{(1)*}, A. Mertens⁽²⁾, H. Kholeif⁽¹⁾, A. Kotz⁽¹⁾, C. Eschenbaum^(1, 2), L. E. Johnson⁽³⁾, D. L. Elder⁽³⁾, S. R. Hammond⁽³⁾, K. O'Malley⁽³⁾, L. Dalton⁽⁴⁾, S. Randel⁽¹⁾, W. Freude⁽¹⁾ and C. Koos^{(1, 2)*}

⁽¹⁾ Inst. of Photonics and Quantum Electron. (IPQ)/Inst. of Microstruct. Technol. (IMT), Karlsruhe Inst. of Technol. (KIT), Germany

⁽²⁾ SilOriX GmbH, Karlsruhe, Germany ⁽³⁾ NLM Photonics, Seattle, USA ⁽⁴⁾ Dpt. of Chemistry, Univ. of Washington, Seattle, USA

*adrian.schwarzeneberger@kit.edu, christian.koos@kit.edu

Abstract We demonstrate the first silicon-organic hybrid electro-optic modulator relying on a long-term-stable thermally crosslinked organic electro-optic material. After more than 2200 hours of high-temperature storage at 120°C, the device still operates at line rates of 200 Gbit/s PAM4 and 100 Gbit/s OOK. ©2023 The Author(s)

Introduction

Hybrid integration of organic materials on silicon or silicon-nitride waveguides allows to combine the intrinsic scalability advantages of the underlying waveguide platform with the wealth of material properties that can be obtained through theory-guided molecular design of organic compounds [1–3]. Specifically, silicon-organic hybrid (SOH) integration has proven particularly promising for high-performance Mach-Zehnder and IQ modulators [4, 5], leveraging organic electro-optic (OEO) materials with in-device Pockels coefficients r_{33} in excess of 300 pm/V [6]. The resulting devices combine sub-1 V π -voltages with device lengths on the order of 1 mm and symbol rates of more than 130 GBd [4, 7] while paving a path towards amplifier-less linear-drive operation with standard CMOS circuits [5, 8]. However, a major shortcoming of the SOH technology is the long-term thermal stability of the electro-optic activity in the OEO material, which relies on an acentric chromophore order established in a one-time poling process during device fabrication. This acentric order needs to be conserved over the lifetime of the device and should be stable against elevated storage and operation temperatures. Previous approaches towards temperature-stable hybrid organic devices relied on OEO materials with high glass-transition temperatures, which were demonstrated to be long-term stable at storage temperatures of up to 90°C [7, 9–11]. While this is an important achievement, operation in a data-center environment requires even higher temperatures. For extension of the temperature range, a promising approach is to use OEO materials that are crosslinked after poling, using appropriate thermally activated [12–14], or photo-activated [15] agents. However, while such crosslinked OEO materials have been used in plasmonic-organic hybrid (POH) electro-optic modulators at temperatures up to 112 °C [16, 17], experimental proofs of long-term temperature thermal stability beyond 85°C were so far limited to thin-film reference samples and did not cover any devices suited for data transmission [13, 14, 16].

In this paper we report on a functional SOH MZM that relies on a crosslinked OEO material and that offers long-term thermal stability at temperatures of 120°C. The material comprises chromophores and thermally activatable crosslinking moieties that allow to con-

serve the acentric chromophore order established during poling. In our experiments, we store the devices for more than 2200 hours at temperatures of 120°C and monitor the evolution of the π -voltage. After an initial increase of the π -voltage, which we attribute to non-crosslinked residuals in the material, we do not observe any significant further degradation of the modulation efficiency. We further show that the MZM still operates at line rates of 200 Gbit/s PAM4 (100 GBd) and 100 Gbit/s OOK after the high-temperature storage. To the best of our knowledge, our experiments correspond to the first experimental demonstration of a functional organic-based modulator that is long-term temperature-stable at temperatures above 100°C. Our device further represents the first SOH modulator that is based on a crosslinked OEO material. We believe that these demonstrations are a key step towards long-term stable hybrid organics-based devices.

Device structure

Figure 1 (a) depicts a schematic of the SOH MZM that is used in our experiments. The device is operated in push-pull configuration with ground-signal-ground (GSG) electrodes. Laser light in the C-band ($\lambda = 1550$ nm) is coupled through grating couplers (GC) to a strip waveguide (WG) and then split into two paths by multi-mode interference (MMI) couplers. In both arms of the MZM, the light is coupled from the strip WG to a slot-WG section and back via strip-to-slot (S2S) converters. A cross-sectional view of the active slot-WG section of the MZM along line A – A in Figure 1 (a) is provided in Figure 1 (b). The slot-WG is formed by two silicon rails (height $h = 220$ nm, width $w = 240$ nm) and a narrow slot in between (width $w_s = 180$ nm), which is filled with the OEO material HLD [13, 14]. The rails are connected to the GSG transmission line by doped silicon slabs (height of $h_{\text{slab}} = 70$ nm). The slabs feature a dedicated multi-level doping profile, in which the region with a high dopant concentration (N^{++} , N^+) remote from the optical WG reduces the ohmic slab resistance, while a low doping (N) level in close vicinity to the slot WG minimizes optical loss [18]. Both the RF and the optical mode are confined to the slot and overlap well, leading

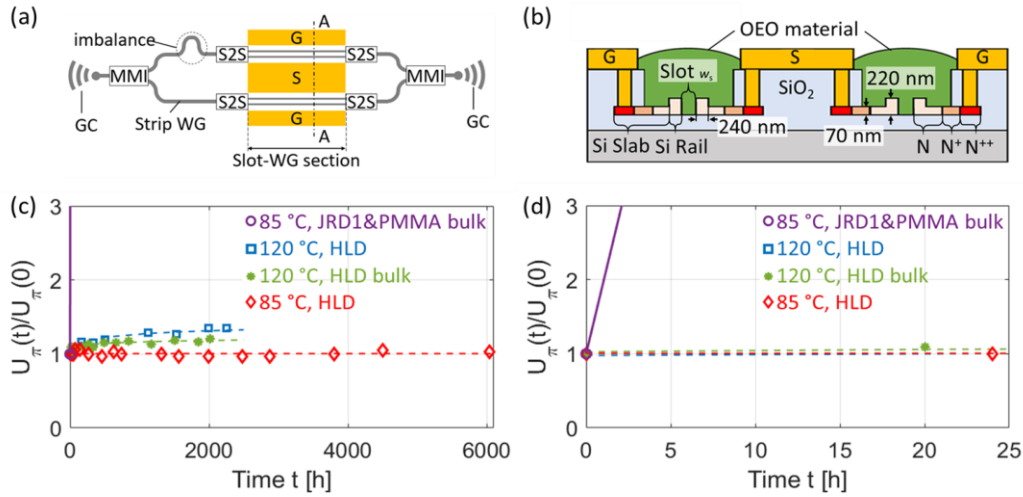


Figure 1: Concept and thermal stability testing of an SOH MZM. **(a)** Top-view schematic of the device: Light is coupled through grating couplers (GC) into a strip WG and split into two optical paths in a multimode interference coupler (MMI). A strip-to-slot (S2S) converter couples the light into the slot-WG section in each arm. The slot is filled with the OEO material HLD. **(b)** Cross-sectional view along the line A – A of the slot-WG section in (a). The slot-WG is formed by two Si rails connected to the ground-signal-ground (GSG) RF transmission line via doped Si slabs and vias. The slabs feature three doping levels (N, N⁺ and N⁺⁺). **(c)** Results of still ongoing thermal in-device stability tests at 120°C and 85°C. The 120°C bulk measurement (green trace) is based on data from [13]. As a reference, the degradation of a 25% JRD1/ PMMA mixture at 85°C is shown in purple with data taken from [14]. **(d)** Magnified view of the initial degradation to illustrate the rapid onset of degradation for the JRD1/PMMA mixture, which loses its entire electro-optic activity within the first 25 hours.

to an EO interaction factor $\Gamma_s = 0.21$, see supplementary information of [19] for details on the definition of Γ_s . The slot-waveguide sections of our devices feature a length of 1 mm. Note that the MZM are designed with unbalanced arm lengths (30 μm mismatch) such that the MZM operating point can be adjusted by proper choice of the wavelength.

Poling, crosslinking, and stability tests

Our demonstrations rely on the two-component thermally crosslinkable OEO material HLD that is described in more detail in [13, 14]. For device preparation, HLD is dissolved in 1,1,2-trichloroethane and manually dispensed onto the silicon photonic base structure of the SOH device. After a pre-crosslinking step, during which the device is heated to 95 °C for an hour, the material is poled by applying a poling field of 147 V/ μm while ramping up the temperature to 145 °C over a period of ten minutes. At this elevated temperature, the OEO material crosslinks, thereby strongly increasing the glass-transition temperature and the thermal stability of the resulting matrix. A π -voltage-length product $U_\pi L$ of 1.9 Vmm was obtained for the 1mm-long device at a wavelength of $\lambda = 1550$ nm, from which we estimate an initial EO coefficient of $r_{33} = 57$ pm/V using the following relation from [19]:

$$U_\pi L = \frac{w_s \lambda}{2n_{\text{EO}}^3 r_{33} \Gamma_s} \quad (1)$$

In this relation, w_s denotes the slot width, and $n_{\text{EO}} = 1.85$ is the refractive index of crosslinked HLD at the wavelength of interest. Note that the Pockels EO coefficient r_{33} of the current device is significantly lower than the 390 pm/V that were previously demonstrated in conventional non-crosslinked materials [6] and that the $U_\pi L$ -product is correspondingly higher. We attribute this to still incomplete poling of the materials during device preparation and expect that this problem can be overcome by further optimizing the material composition, the poling, and the crosslinking procedures.

To characterize the thermal stability of the devices, storage tests at elevated temperatures were conducted. These tests were performed in vacuum to isolate de-poling from other chemically induced degradation processes [13, 14, 16]. These degradation processes can alternatively be mitigated by introducing a protective encapsulation layer [16]. After initial characterization of the devices, one batch of modulators was stored for more than 6000 hours at 85°C. The time-dependent evolution of the π -voltage U_π normalized to its initial value is shown as a red trace in Figure 1 (c). The data does not exhibit any degradation over the entire experiment. For comparison, the degradation of a bulk sample taken from [14] featuring a thin film of 25% JRD1 with polymethylmethacrylate (PMMA) is shown in purple. After a day of high temperature storage, the electro-optic activity of the device degrades by a factor of 20. To make the rapid degradation more apparent Figure 1 (d) depicts only the first 25 hours of the storage experiment.

The second batch of devices was stored at 120°C. This test was started with a delay of approximately 3800 h with respect to the 85°C test series, such that only approximately 2200 h of test history were available at manuscript submission – the experiment is being continued. The normalized in-device π -voltage, represented by the blue trace in Fig. 1(c), increased by a factor of approximately 1.27 with respect to its initial value within the first 1000 h and then seems to settle – after 2000 h, the π -voltage has increased only slightly to 1.30 times the initial value. As a reference, we also show the normalized degradation of the reciprocal of the electro-optic coefficient r_{33} of HLD bulk material at 120°C in N_2 atmosphere [13], see green trace in Fig. 1(c). An initial degradation by a factor of 1.18 can be observed within the first 1000 h, and the performance seems to be stable afterwards. We attribute the initial degradation of bulk and in-device samples stored at 120°C to residual chromophores that are only

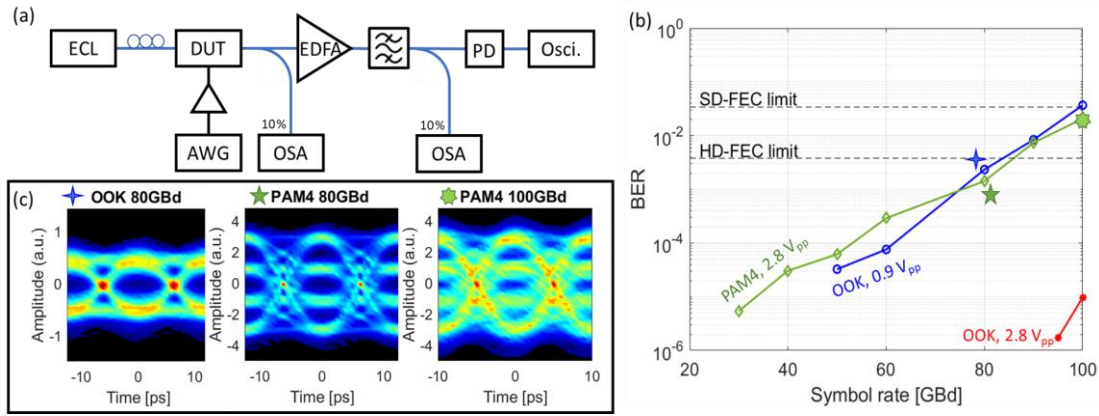


Figure 2: Data transmission experiment using an SOH MZM with HLD as EO material aged for 2256 hours at 120°C in vacuum. **(a)** Schematic of the setup: An external-cavity laser (ECL) is coupled to the device under test (DUT) using fiber probes. The drive signal is provided by an arbitrary-waveform generator (AWG) and amplified by an 11 dB RF amplifier. The modulated light is coupled to an erbium-doped fiber amplifier (EDFA) via a fiber probe. A tunable optical filter is used to suppress amplified spontaneous emission. The light is detected by a photodetector (PD) and the waveform is recorded using a real time oscilloscope (Osci.). **(b)** Resulting bit error ratio (BER) vs. symbol rate for OOK and PAM 4 signaling. For OOK, two sweeps with a nominal drive voltage of 0.9 V_{pp} and 2.8 V_{pp} were recorded (blue and red lines respectively). For PAM4, the nominal drive voltage was set to 2.8 V_{pp}, and the resulting curve is shown in green. The black dashed line depicts both the Soft-decision (SD-FEC) and hard-decision (HD-FEC) forward error coding limit. **(c)** Eye diagrams for PAM4 at symbol rates of 80 GBd and 100 GBd and OOK at 80 GBd as highlighted in (b).

weakly bound to the crosslinked matrix, and we believe that further optimizing the material composition and the crosslinking will eliminate this effect. Similarly, the increased in-device degradation compared to HLD in bulk is attributed to the lower crosslinking temperature of 145°C as compared to 155°C used for the bulk samples – also here, further process optimization might overcome this problem. We further investigated the optical loss before and after storage at 120°C and did not find any significant changes.

Data Transmission Experiment

To prove the functional stability of the device, we perform data-transmission experiments using the devices at the end of the high-temperature storage test (2256 h @ 120°C) using the setup shown in Figure 2 (a). An external-cavity laser (ECL) is connected to the device under test (DUT) via fiber probes and grating couplers. The drive signal for the DUT is provided by a Keysight M8194A arbitrary-waveform generator (AWG) and amplified by an 11 dB RF amplifier. At the output of the modulator, the signal is coupled to a fiber and amplified by an erbium-doped fiber amplifier (EDFA) to 10.5 dBm. A tuneable bandpass filter with a bandwidth of 3 nm is used to suppress amplified spontaneous emission noise from the EDFA. After the filter, the light is coupled to a photodetector (PD), and the resulting waveform is captured with a Keysight UXR1004A high-speed real time oscilloscope (Osci.). Two 10 % taps after the DUT and the filter are used to monitor transmission and to adjust the optical filter. An offline digital signal processing chain consisting of resampling, timing recovery, and a Sato equalizer is applied to the captured waveform, and the bit-error ratio (BER) is measured. Both OOK and PAM4 were transmitted. In case of PAM4, an additional decision-directed least-mean-square equalizer with 151 taps is used.

The BER for various symbol rates is depicted in Figure 2 (b) for OOK and PAM4. In case of OOK, two different nominal peak-to-peak drive voltages, 2.8 V_{pp} and 0.9 V_{pp}, are set at the output of the RF amplifier. Note that the voltage effective at the device is slightly lower

due to the attenuation of the RF cable and the frequency-dependent decay of the transfer function of the probe. As an example, at 100 GBd PAM4, the on-chip drive voltage was estimated to be 2.1 V_{pp}.

For a nominal drive voltage of 2.8 V_{pp}, the OOK BER (red trace) is below the threshold for hard-decision forward error correction (HD-FEC) with 7% overhead. At a nominal drive voltage of 0.9 V_{pp}, the OOK BER (blue curve) is still below the HD-FEC limit for a maximum symbol rate of 80 GBd. The corresponding eye diagram is to be seen in Figure 2 (c). For PAM4 signalling at a nominal drive voltage of 2.8 V_{pp} (green trace), the BER for a symbol rate (line rate) of up to 80 GBd (160 Gbit/s) stays below the HD-FEC limit, while the BER for a symbol rate (line rate) of 100 GBd (200 Gbit/s) still remains below the SD-FEC limit. The corresponding eye diagrams are shown in Figure 2 (c). These experiments show that the functionality of the device is maintained even after storage for more than 2200 h at a temperature of 120 °C.

Summary

We have demonstrated the first silicon-organic hybrid (SOH) Mach-Zehnder modulator that relies on a thermally crosslinked organic electro-optic (OEO) material. We store test devices for 6000 h at 85 °C and for 2200 h at 120°C. At 85°C, we do not observe any degradation, while an initial increase of the π -voltage by approximately 30 % and a settling of the device performance afterwards is observed at 120°C. We believe that the initial degradation can be avoided by further optimizing the material composition and the crosslinking process. Using the thermally aged device, we demonstrate 100 GBd PAM4 transmission below the SD-FEC limit with 20 % coding overhead. To the best of our knowledge, our experiments correspond to the first experimental demonstration of a functional organics-based modulator that is long-term thermally stable at temperatures of more than 90°C. We believe that our demonstrations pave a path towards long-term stable hybrid organic-based devices that can offer various advantages in terms of scalability and performance.

Acknowledgements

This research has been funded by the European Research Council (ERC Consolidator Grant “TeraSHAPE”, 773248), by the EU project “TeraSlice” (# 863322) and DYNAMOS (# 101070342), by the Deutsche Forschungsgemeinschaft (DFG, German Research Foundation) via the projects PACE (# 403188360) and GOSPEL (# 403187440), via the DFG Collaborative Research Center (CRC) HyPERION (SFB 1527, # 454252029), and via the Excellence Cluster 3D Matter Made to Order (EXC-2082/1 – 390761711), by the BMBF projects Open6GHub (16KISK010) and INTERSOUL (16KISK244K), by the Karlsruhe School of Optics & Photonics (KSOP), and by the Alfred Krupp von Bohlen und Halbach Foundation.

References

- [1] L. Dalton and S. Benight, “Theory-Guided Design of Organic Electro-Optic Materials and Devices,” *Polymers*, vol. 3, no. 3, pp. 1325–1351, Aug. 2011, doi: 10.3390/polym3031325.
- [2] C. Koos *et al.*, “Silicon-Organic Hybrid (SOH) and Plasmonic-Organic Hybrid (POH) Integration,” *J. Lightwave Technol.*, vol. 34, no. 2, pp. 256–268, Jan. 2016, doi: 10.1109/JLT.2015.2499763.
- [3] D. Kohler *et al.*, “Biophotonic Sensors with Integrated Si₃N₄-Organic Hybrid (SiNOH) Lasers for Point-of-Care Diagnostics,” *Light Sci Appl*, vol. 10, no. 1, p. 64, Mar. 2021, doi: 10.1038/s41377-021-00486-w.
- [4] S. Wolf *et al.*, “Coherent Modulation up to 100 GBd 16QAM using Silicon-Organic Hybrid (SOH) Devices,” *Optics Express*, vol. 26, no. 1, pp. 220–220, 2018, doi: 10.1364/oe.26.000220.
- [5] C. Kieninger *et al.*, “Silicon-Organic Hybrid (SOH) Mach-Zehnder Modulators for 100 GBd PAM4 Signaling with sub-1 dB Phase-Shifters Loss,” *Opt. Express*, vol. 28, no. 17, p. 24693, Aug. 2020, doi: 10.1364/OE.390315.
- [6] C. Kieninger *et al.*, “Ultra-High Electro-Optic Activity Demonstrated in a Silicon-Organic Hybrid Modulator,” *Optica*, vol. 5, no. 6, pp. 739–739, 2018, doi: 10.1364/optica.5.000739.
- [7] C. Eschenbaum *et al.*, “Thermally Stable Silicon-Organic Hybrid (SOH) Mach-Zehnder Modulator for 140 GBd PAM4 Transmission with Sub-1 V Drive Signals,” in *European Conference on Optical Communication (ECOC) 2022*, Optica Publishing Group, 2022, p. Th3B.2. [Online]. Available: <https://opg.optica.org/abstract.cfm?URI=ECEOC-2022-Th3B.2>
- [8] S. Wolf *et al.*, “DAC-less Amplifier-less Generation and Transmission of QAM Signals using Sub-Volt Silicon-Organic Hybrid Modulators,” *Journal of Lightwave Technology*, vol. 33, no. 7, pp. 1425–1432, 2015, doi: 10.1109/JLT.2015.2394511.
- [9] C. Kieninger *et al.*, “Demonstration of Long-Term Thermally Stable Silicon-Organic Hybrid Modulators at 85 °C,” *Optics Express*, vol. 26, no. 21, pp. 27955–27955, 2018, doi: 10.1364/oe.26.027955.
- [10] G.-W. Lu *et al.*, “High-Temperature-Resistant Silicon-Polymer Hybrid Modulator Operating at up to 200 Gbit s⁻¹ for Energy-Efficient Datacentres and Harsh-Environment Applications,” *Nat Commun*, vol. 11, no. 1, p. 4224, Aug. 2020, doi: 10.1038/s41467-020-18005-7.
- [11] M. Eppenberger *et al.*, “Resonant Plasmonic Micro-Racetrack Modulators with high Bandwidth and high Temperature Tolerance,” *Nat. Photon.*, vol. 17, no. 4, pp. 360–367, Apr. 2023, doi: 10.1038/s41566-023-01161-9.
- [12] Z. Zeng *et al.*, “Electro-Optic Crosslinkable Chromophores with Ultrahigh Electro-Optic Coefficients and Long-Term Stability,” *Chem. Sci.*, vol. 13, no. 45, pp. 13393–13402, 2022, doi: 10.1039/D2SC05231H.
- [13] S. R. Hammond, K. M. O’Malley, H. Xu, D. L. Elder, and L. E. Johnson, “Organic Electro-Optic Materials Combining Extraordinary Nonlinearity with Exceptional Stability to enable Commercial Applications,” in *Organic Photonic Materials and Devices XXIV*, I. Rau, O. Sugihara, and W. M. Shensky, Eds., San Francisco, United States: SPIE, Mar. 2022, p. 35. doi: 10.1117/12.2622099.
- [14] H. Xu *et al.*, “Ultrahigh Electro-Optic Coefficients, High Index of Refraction, and Long-Term Stability from Diels–Alder Cross-Linkable Binary Molecular Glasses,” *Chem. Mater.*, vol. 32, no. 4, pp. 1408–1421, Feb. 2020, doi: 10.1021/acs.chemmater.9b03725.
- [15] M. Tamilvanan, A. Pandurangan, B. S. Reddy, and K. Subramanian, “Synthesis, Characterization and Properties of Photoresponsive Polymers comprising Photocrosslinkable Pendant Chalcone Moieties,” *Polym. Int.*, vol. 56, no. 1, pp. 104–111, Jan. 2007, doi: 10.1002/pi.2124.
- [16] C. Hoessbacher *et al.*, “Plasmonic-Organic-Hybrid (POH) Modulators - a Powerful Platform for Next-Generation Integrated Circuits,” in *OSA Advanced Photonics Congress 2021*, Washington, DC: Optica Publishing Group, 2021, p. IW1B.5. doi: 10.1364/IPRSN.2021.IW1B.5.
- [17] U. Koch *et al.*, “A Monolithic Bipolar CMOS Electronic–Plasmonic High-Speed Transmitter,” *Nat Electron*, vol. 3, no. 6, pp. 338–345, Jun. 2020, doi: 10.1038/s41928-020-0417-9.
- [18] H. Zwickel *et al.*, “Verified Equivalent-Circuit Model for Slot-Waveguide Modulators,” *Opt. Express* 28, pp. 12951–12976, 2020, doi: 10.1364/OE.383120
- [19] S. Ummethala *et al.*, “Hybrid electro-optic modulator combining silicon photonic slot waveguides with high-k radio-frequency slotlines,” *Optica*, vol. 8, no. 4, pp. 511–511, Apr. 2021, doi: 10.1364/optica.411161.